Journal of the Optical Society of Korea, Vol. 11, No. 4, December 2007, pp. 162-172

Maximizing the Workspace of Optical Tweezers

Sun-Uk Hwang and Yong-Gu Lee*

Department of Mechatronics, Gwangju Institute of Science and Technology (GIST), Gwangju, 500-712, Korea

(Received October 30, 2007 : revised November 26, 2007)

Scanning Laser Optical Tweezers (SLOT) is an optical instrument frequently employed on a microscope with laser being delivered through its various ports. In most SLOT systems, a mechanical tilt stage with a mirror on top is used to dynamically move the laser focal point in two-dimensions. The focal point acts as a tweezing spot, trapping nearby microscopic objects. By adding a mechanical translational stage with a lens, SLOT can be expanded to work in three-dimensions. When two mechanical stages operate together, the focal point can address a closed three-dimensional volume that we call a workspace. It would be advantageous to have a large workspace since it means one can trap and work on multiple objects without interruptions, such as translating the microscope stage. However, previous studies have paid less consideration of the volumetric size of the workspace. In this paper, we propose a new method for designing a SLOT such that its workspace is maximized through optimization. The proposed method utilizes a matrix based ray tracing method and genetic algorithm (GA). To demonstrate the performance of the proposed method, experimental results are shown.

OCIS codes : 080.0080, 080.2720, 080.2730, 080.2740

I. INTRODUCTION

Optical Tweezers (OT) are widely used as a tool for manipulating microscopic objects, or measuring pico-Newton forces in biological objects [1-5]. The principle of optical trapping is that particles are attracted to the focal point of a laser beam by the conservation of momenta [6-7]. This means by controlling the position of the focal point, particles can be position controlled. There are many methods to move the focal point. One of the oldest ways of moving the focal point is by the use of rapidly tilting mirrors and translating lenses [8]. The family of OT utilizing this method is called SLOT and it has been widely adopted by many researchers [8-13]. To control the position of a focal point, SLOT uses a motorized tilt stage and a motorized translational stage. Motorized tilt stage with a mirror on top can be used to deflect beams and motorized translational stage with a lens can be used to change the convergence/divergence angle of a beam. From here on, these motorized assemblies will be denoted as "motorized mirrors" and "motorized lenses." These devices can move the focal point very rapidly enabling one to devise multiple traps [9,11]. At present, with the advance of piezo electric systems, tilt stage that incorporates piezo actuator can move the focal point laterally much faster than a motorized tilt stage, reaching a frequency of 10^6 Hz [9].

Figure 1(a) illustrates a layout of a typical SLOT. When a motorized lens and a motorized mirror dynamically translate and rotate, the laser focus can address a closed volume that we call a workspace. For example in Fig. 1(a), clockwise rotation of the motorized mirror around the positive y-axis and motion of the motorized lens in the positive x-axis results in the focal point reaching point 1. Similarly, counterclockwise rotation of the motorized mirror around the negative y-axis and motion of the motorized lens in the negative x-axis results in the focal point reaching point 2. The motorized mirror can also rotate around z'-axis and this enables the focal point to address points below points 1 and 2 in Fig. 1(a).

In micro manipulation, it is crucial to have a large workspace because it provides a wider range of control of single trapped objects and the ability to simultaneously trap multiple objects that are far apart. However, previous studies have paid less consideration of the volumetric size of the workspace. Furthermore, when high speed scanning actuators are used, the moving range decreases, resulting in a smaller workspace [14]. For these reasons, the workspace is frequently much smaller than the field of view of the microscope. Small

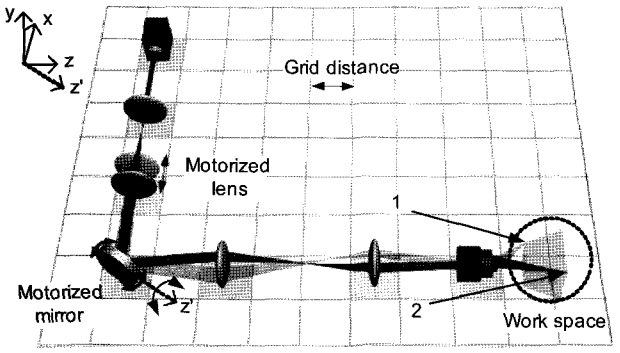

(a) Scanning laser optical tweezers

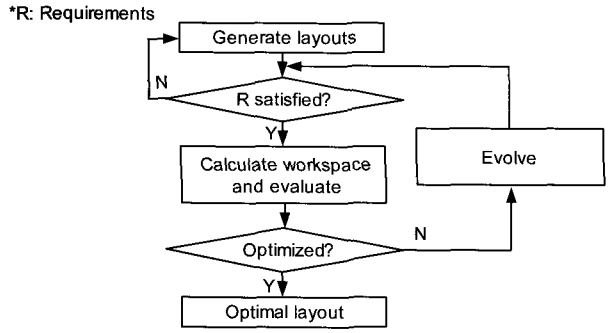

(b) Maximizing the workspace with GA

FIG. 1. Schematic description of this study.

workspace requires the microscope stage to be moved when objects escape from the workspace. This makes it difficult to operate on multiple objects such as assembling multiple components together.

At first look, it would seem easy to accomplish the task of maximizing the workspace. This is partly true if one does not care much about the laser power. However, careless design layout would result in an inefficient use of the laser power. The principal behind high efficiency is simple. When the laser beam reaches the objective back aperture (OBA), the circular beam cross section should closely match the aperture. In this way, full beam power gets transmitted to the focal point. However, this is not a simple task in SLOT because during operations, cross section of a beam often deviates far away from the central axis. The solution to this problem has been suggested by Fallman *et al.* [8] and Mio *et al.* [9]. SLOT should be designed such that the laser beam overfills at the objective back aperture (OBA) and pivots around the center of the OBA. When these two constraints are met, maximum efficiency is achieved. However, with these constraints alone, optimized design that gives maximized workspace cannot be determined. According to the selection of several design parameters such as number of optical elements, focal lengths of lenses and positions of optical elements, there could be many design solutions with different workspaces to meet the above constraints.

To resolve this problem, we propose a new method for designing an optimized SLOT that gives maximized workspace with a given pool of optical elements. To find out the best layout that is optimized for various design parameters, GA was used. GA is widely used for the design optimization of optical elements such as lens [15,16], polarizer [16], photonic crystal fiber [17], diffractive optical element [18]. GA utilizes the fact that life forms that adapt to nature give more offspring, and evolution is achieved through the change of chromosomes. This is a computational technique which is used to solve the problems where there are many potential solutions but a small number of optimal solutions. The strength of this method is that it does not require a differentiation of the objective function. Instead, GA stochastically searches the global solution in parallel using all the variables in the objective function [19]. Fig. 1(b) illustrates the optimization process in finding the optimal layout that maximizes workspace. In the beginning, we first divide the layout space into finite grids where two consecutive grids have a finite distance denoted as a grid distance and then randomly distribute lenses and mirrors to appropriate grids. One layout forms one configuration and this is represented by a chromosome. Multiple chromosomes form one population. Subsequently, each chromosome in a population is tested to see if it satisfies the requirements. If the test is successful, the layout (chromosome) and its performances are recorded. This concludes one step and for the next iteration the population goes through evolution. During each step, it is checked if termination conditions are met. At the end, the best performing layout is found.

This paper is structured as follows: In Section II, we derive objective function and requirement equations. In Section III, we introduce a chromosome that describes one layout. Crossover and mutation are used to evolve a population of chromosomes. In Section IV, we show the optimization result that gives the maximum workspace by varying the number of optical elements and the grid distance between optical elements. Finally, in Section V, we conclude this paper by summarizing our results.

II. OBJECTIVE FUNCTION AND REQUIREMENT EQUATIONS

Lenses and mirrors in an optical system change the height and angle of incoming beam. These changes can be expressed in matrices. By combining these matrices from each lens and mirror, a system matrix (S) can be formed that relates the incoming beam to the exiting beam [20]. Appendix A derives the system matrix for our SLOT. Using the system matrix, we can derive the objective function whose value is the workspace volume.

This is given in Section II.1. In Section II.2, requirement equations that need to be satisfied while maximizing the objective function are derived. For the derivation, we assume that there are negligible aberrations in the system. We also assumed that the curvature field in the sample specimen that results from tilt mirror scanning is flat, since the radius of curvature by lateral scanning is very large.

II.1. Derivation of objective function

For practical reasons, we only allow one motorized mirror and one motorized lens with other elements fixed by holders. Figure 2 illustrates one dimensional representation of SLOT when a motorized lens is translated and a motorized mirror is rotated.

Figure 2(a-c) show three modes where each mode describes different positions of focal points. Mode I corresponds to the situation when the motorized lens is at its neutral position and the motorized mirror is rotated at $+\phi$ or $-\phi$. Similarly, Mode II and Mode III are when the motorized lens is at $-\delta$ and $+\delta$, respectively, with the motorized mirror rotated at $+\phi$ and $-\phi$. And Fig. 2(d) shows schematic view of SLOT to derive longitudinal displacement and lateral displacement of the focal point. This is an example when a motorized lens is moved to the right and a motorized mirror is rotated to the counter clockwise direction. In the figure, subscript $k(0\sim n)$ denotes the index of the k th element. C_0 and C_n are a laser source and an objective lens, respectively. $C_1\cdots C_{n-1}$ are optical elements consisting of lenses and mirrors. C_l and C_m denote a motorized lens and a motorized mirror, respectively. $\bar{z}_k$ denotes the position of the k th element at the neutral state. The neutral state is defined as the state when all the motorized elements are at the middle of their dynamic movement ranges. At the neutral state, the upper and lower beam heights at each optical element are the same.

However, when motorized elements move, the upper and lower beam heights are different. We thus introduce a new notation to differentiate the upper and lower beam heights. We will use '^' to denote lower beam height. For example, if the upper beam height at the k th optical element is h_k, the lower beam height will be represented as $\hat{h}_k$. Similar to the axial positions at the neutral state, we will use a bar '-' to represent the height at the neutral state. For example, the upper

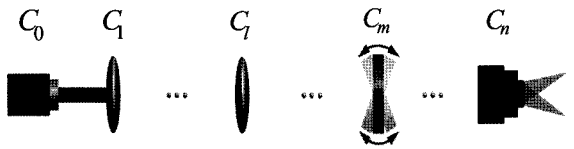

(a) Mode I (Motorized lens is at neutral position and motorized mirror rotates.)

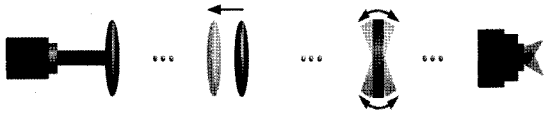

(b) Mode II (Motorized lens moves to the left and motorized mirror rotates.

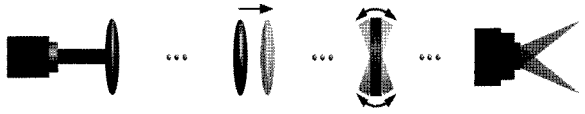

(c) Mode III (Motorized lens moves to the right and motorized mirror rotates.)

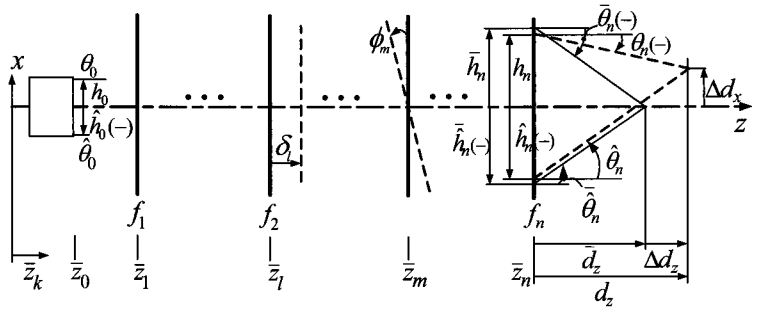

(d) Motorized lens moves to the right and motorized mirror rotates to the ccw

FIG. 2. Schematic view of SLOT when a motorized lens is translated and a motorized mirror rotated.

beam height of the k th optical element at neutral state will be $\bar{h}_k$. The decorations can be combined, thus the lower beam height of the k th optical element at the neutral state will be $\hat{\bar{h}}_k$. Similarly, upper beam angles of the k th optical element are represented as θ_k and same rules are applied for neutral and lower decorations for beam angles. Lastly, f_k, δ_l and ϕ_m denote focal length of the k th optical element, motorized translation distance and motorized rotation angle, respectively. Our sign convention is positive when a vector is upwards and a rotation is counterclockwise. Here, we can calculate the relative position of the focal point respective to the OBA at the neutral state as

$$\bar{d}_z = \bar{h}_n / \tan\bar{\theta}_n = \bar{h}_n / \bar{\alpha}_n, \ \textit{where} \ \ \bar{\alpha}_n = \tan\bar{\theta}_n. \tag{1}$$

The new position of the focal point in the z direction when motorized elements move and rotate is (see Appendix B)

$$d_z = \frac{h_n + \hat{h}_n}{\alpha_n + \hat{\alpha}_n}, \ \textit{where} \ \ \alpha_n = \tan\theta_n \ \text{and} \ \hat{\alpha}_n = \tan\hat{\theta}_n. \tag{2}$$

Thus the longitudinal displacement in the z direction is

$$\Delta d_z = d_z - \bar{d}_z = G(\phi_m, \delta_l, f_1, \cdots, f_n, \bar{z}_0, \bar{z}_1, \cdots \bar{z}_{n-1}, \bar{z}_n). \tag{3}$$

The lateral displacement in the x direction perpendicular to the beam axis can be derived as

$$\Delta d_x = \frac{h_n\hat{\alpha}_n - \hat{h}_n\alpha_n}{\alpha_n + \hat{\alpha}_n} = H(\phi_m, \delta_l, f_1, \cdots, f_n, \bar{z}_0, \bar{z}_1, \cdots \bar{z}_{n-1}, \bar{z}_n). \tag{4}$$

Above derivations are the same with the lateral displacement in the y direction because typical tilt stage is manufactured to have same rotation angle for two different axes. This makes the shape of the cross-section of the workspace, square. Notice we zeroed out all motorized angles and motorized displacements except those of the motorized mirror and the motorized lens because we only allow one motorized lens and one motorized mirror. The volume of the workspace can be calculated by using Δd_z and Δd_x according to the three modes described in Fig. 2. By assuming the focus plane by laser scanning is flat, the shape of workspace can have four types whose workspace can be represented as the shape obtained by adding two frustums W_1 and W_2 as illustrated in Fig. 3.

Here, $\Delta d_x\big|_{\delta_l=0,\phi_m=\pm\phi}$, $\Delta d_x\big|_{\delta_l=-\delta,\phi_m=\pm\phi}$ and $\Delta d_x\big|_{\delta_l=+\delta,\phi_m=\pm\phi}$ are the lateral displacements of Mode I, Mode II and Mode III, respectively. $\Delta d_z\big|_{\delta_l=-\delta,\phi_m=0}$ and $\Delta d_z\big|_{\delta_l=+\delta,\phi_m=0}$ are the longitudinal displacements of Mode II and Mode III, respectively. By defining following three average values,

$$L_I = \frac{\Delta d_x\big|_{\delta_l=0,\phi_m=+\phi} - \Delta d_x\big|_{\delta_l=0,\phi_m=-\phi}}{2}$$

$$L_{II} = \frac{\Delta d_x\big|_{\delta_l=-\delta,\phi_m=+\phi} - \Delta d_x\big|_{\delta_l=-\delta,\phi_m=-\phi}}{2}$$

$$L_{III} = \frac{\Delta d_x\big|_{\delta_l=+\delta,\phi_m=+\phi} - \Delta d_x\big|_{\delta_l=+\delta,\phi_m=-\phi}}{2}$$

the volume of the workspace is thus

$$\begin{aligned} W = W_1 + W_2 &= \frac{4}{3}\left[\begin{array}{l}\left(\Delta d_z\big|_{\delta_l=-\delta,\phi_m=0}\right)\left\{(L_I)^2 + L_I L_{II} + (L_{II})^2\right\} \\ +\left(\Delta d_z\big|_{\delta_l=+\delta,\phi_m=0}\right)\left\{(L_I)^2 + L_I L_{III} + (L_{III})^2\right\}\end{array}\right] \\ &= W(f_1, \cdots, f_n, \bar{z}_0, \bar{z}_1, \cdots \bar{z}_{n-1}, \bar{z}_n, l). \end{aligned} \tag{5}$$

W is a function of focal lengths, element positions and the index of the motorized lens. Index of motorized mirror is implicitly noted by one of the focal lengths that is ∞.

II.2. Requirements equations

In addition to the objective function, we need to satisfy several requirement equations to create a movable trap that is efficient and stable regardless of the movement of the beam. These equations should be checked while maximizing the objective function. Firstly, the laser beam must rotate while pivoted at the center of OBA. This is realized by,

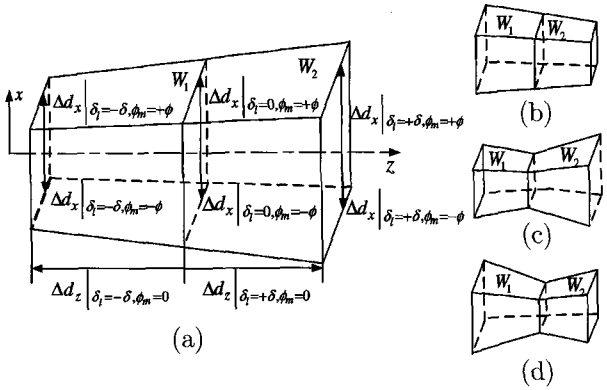

FIG. 3. Shape of the workspace (The shape of the cross-section of the workspace is planar-square by the assumption that the focus plane by laser scanning is flat.).

$$-\varepsilon \le \frac{h_n + \hat{h}_n}{2} \le \varepsilon, \tag{6}$$

where ε is a tolerance value for length. Secondly, the laser beam must overfill the OBA to sustain same amount of trapping power even if the beam is moved. This can be represented by,

$$r_n(1-\varepsilon) \le \frac{h_n - \hat{h}_n}{2} \le r_n(1+\varepsilon), \tag{7}$$

where r_n is the radius of the objective lens. Thirdly, the beam height should not be greater than the optical element's physical dimension. This is enforced by the following two inequalities,

$$h_k \le r_k, \ \hat{h}_k \ge -r_k, \tag{8}$$

where r_k is the radius of the k th optical element. Fourthly, there should be a minimum spacing between two adjacent optical elements. This requirement is stated as

$$\bar{z}_k - \bar{z}_{k-1} \ge \Delta\bar{z}. \tag{9}$$

Lastly, all optical elements should be placed within the maximum length of the total beam path, z_{max}, that is determined by the size of the optical table. This requirement is stated as

$$z_k \le z_{\max}. \tag{10}$$

III. MAXIMIZING WORKSPACE

The first step of GA is the initialization of a population. At this stage, potential optical layouts are randomly generated to constitute the initial population. Subsequently, from this initial population, only the chromosomes that satisfy the requirements in section II.2 survive and are evaluated by the objective function in Eq. (5). Lastly, evolution procedure composed of selection, crossover and mutation is performed to search for the optimized chromosome that maximizes the objective function. The optimized chromosome corresponds to the optimized SLOT layout that maximizes the workspace.

III.1. Chromosomes

As we derived in section II, the objective function for proposed SLOT system is a function of focal lengths, neutral state locations of optical elements and the index of motorized lens. This function is used to evaluate individual optical layout which denotes chromosome. Figure 4 illustrates the representation of chromosomes. A chromosome consists of values that uniquely determine an optical layout. Member values of a chromosome are a series of focal lengths, neutral state locations of optical elements and the index of motorized lens. Index of the motorized mirror is not explicitly used. This is redundant information because among the optical elements, the one that has infinite focal length denotes the motorized mirror. Chromosomes are represented as real values as opposed to the binary string common in genetic algorithm.

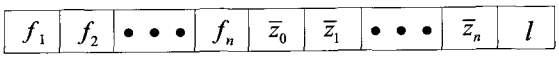

FIG. 4. A chromosome that composed of element variables.

III.2. Crossover and mutation

In this subsection, we briefly give an example for crossover and mutation. Figure 5 shows crossover and mutation of chromosomes when n is six. The variables that constitute a chromosome are as follows. (f_1, f_2, f_3, f_4, f_5, f_6) and (f_1', f_2', f_3', f_4', f_5', f_6') are focal lengths. ($\bar{z}_0$, $\bar{z}_1$, $\bar{z}_2$, $\bar{z}_3$, $\bar{z}_4$, $\bar{z}_5$, $\bar{z}_6$) and ($\bar{z}_0'$, $\bar{z}_1'$, $\bar{z}_2'$, $\bar{z}_3'$, $\bar{z}_4'$, $\bar{z}_5'$, $\bar{z}_6'$) are element positions. l, l' are the indices of motorized lenses. Figure 5(a) shows crossover. (cp_1, cp_2, cp_3, cp_4, cp_5, cp_6) denote crossover points. Each population has probability of crossover. We used 25%. When performing the crossover, the remaining 75% is generated again by crossover from this 25%. Original 75% not participating in the crossover are removed. Crossover is achieved by swapping the variables between odd and even crossover points. This process makes two new chromosomes from the previous two chromosomes. However, only one chromosome is selected and used. The selection is random and the other chromosome is removed.

Figure 5(b) shows mutation. Here, (mp_1, mp_2, mp_3, mp_4) denote mutation points and (f_3^*, $\bar{z}_2^*$, l^*) represent variables that are mutated. We only mutate three variables. Those are one from each set of focal lengths, element positions and index of motorized lens. Mutation is accomplished by changing variables according to the mutation probability. Either after the crossover or mutation, there can be situations when there are more than one focal length that have the value of ∞. This is not acceptable because we only allow one mirror. Thus after each operation, all focal lengths are examined. And if more than one focal length has the value of ∞, only one is kept untouched while others are converted to new focal lengths. The new focal lengths are chosen randomly.

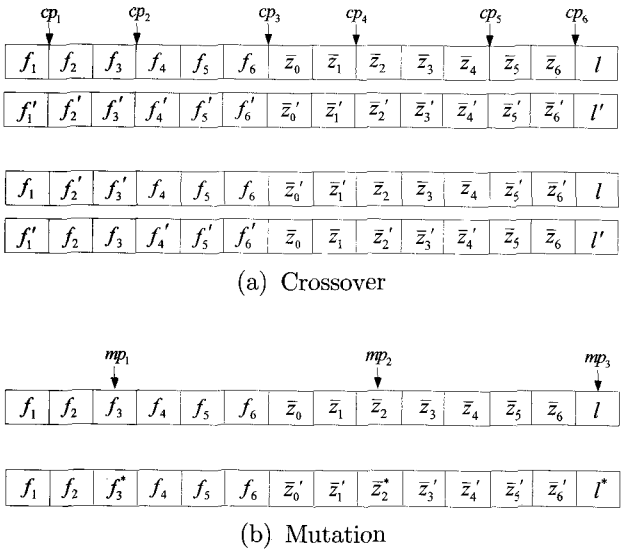

(a) Crossover

(b) Mutation

FIG. 5. Crossover and mutation when n is six.

III.3. Values used for the examples

Examples are run with several constant and variable values determined by the specifications of optical elements. All the specifications of lenses, mirrors and the objective lens described are from commercially available optical elements. We briefly describe the constant values that we used in Table 1.

Incoming laser beam $\mathbf{l}_0$ is a collimated laser beam with diameter of 5 millimeters. The maximum length of the optical layout z_{max} is bound by 1500 millimeters. The minimum spacing $\Delta\bar{z}$ between adjacent optical elements is set to 50 millimeters. The radii of optical elements r_k ($k = 1, \cdots, n\text{-}1$) are set to a uniform size of 25.4 mm. The OBA radius r_n is set to 1.8 millimeters. The maximum amplitudes of rotations and translations are chosen from commercially available actuators. They are 10 milliradians for ϕ and 50 mm for δ. The length tolerance ε is 0.01. And constant values that drive the optimization are described in Table 1b). The size of a population is set by POPSIZE. To avoid the infinite loop in the optimization, MaxGen limits the maximum number of generations allowed. The probability of crossover and mutation are set to 0.25 and 0.05, respectively. Table 2 lists variable values for chromosome constitution. Variable values are composed of the number of optical elements (n) excluding the laser source, focal lengths (f_k), positions ($\bar{z}_k$) and the index of the motorized lens (l). f_k is selected from the pool of available focal lengths. Infinite (∞) and 1.82 are set to the focal length of the mirror and the objective lens, respectively. All optical elements at the neutral state are placed at grid points separated by 5 mm. Index of the motorized lens (l) can have positive value less than n.

TABLE 1. Constant values for implementation

(a) Constant values for optical elements (mm, mrad)

I_0	z_{max}	$\Delta\bar{z}$	$r_k(k=1,\cdots,n\text{-}1)$	r_n	$\delta_{\max}$	$\phi_{\max}$	ε
$h_0 = -\hat{h}_0 = 2.5$ $\alpha_0 = \hat{\alpha}_0 = 0$	1500	50	25.4	1.8	50	10	0.01

(b) Constant values for GA

POPSIZE	MaxGen	Probabilty of Crossover	Probabilty of Mutation
200,000	500	0.25	0.05

TABLE 2. Available values for chromosome constitution (mm)

f_k	$\bar{z}_k$	l
{∞,60, 100, 120, 150, 180, 200, 250,1.82}	1500	[1, n-1]

IV. OPTIMIZATION RESULTS AND DISCUSSIONS

Figure 6 shows the graph of the best fitness as new generations are formed. Each graph is a result obtained by varying n from five to ten. In Fig. 6(a), solid line denotes the case when n is 5; dash-dot line is the case when n is six and dotted line shows the case when n is seven. In Fig. 6(b), solid line denotes the case when n is eight; dash-dot line is the case when n is nine and dotted line shows the case when n is ten. Fitness is the size of the workspace determined by each chromosome. We use fitness instead of workspace because it is a common terminology used in the GA community. GA saves the chromosome that gives the best fitness in each generation. This is why the best fitness increases monotonously. In the figure, GA converges at the generation approximately less than 260 for all cases of n. When the optimal chromosome is found, we see no increase in the best fitness. Examining Fig. 6, we can see that the case when n is ten shows the maximum best fitness which gives the best layout that maximizes the workspace.

Table 3 summarizes the best chromosomes obtained by varying n from five to ten. In the table, laser source is located at zero position and location of the motorized mirror is denoted by the infinite value in the focal length. Index of motorized lens is denoted by l. This is the optimal solution for given n.

All the data from here are obtained from the case when the grid distance of optical elements is 5 mm. To verify the validity of the grid distance of optical elements, we execute the same procedure for the cases when the grid distance of optical elements is 10 mm, 2.5 mm and 0.5 mm. Table 4 shows the optimal solutions for the cases when n is ten with different grid

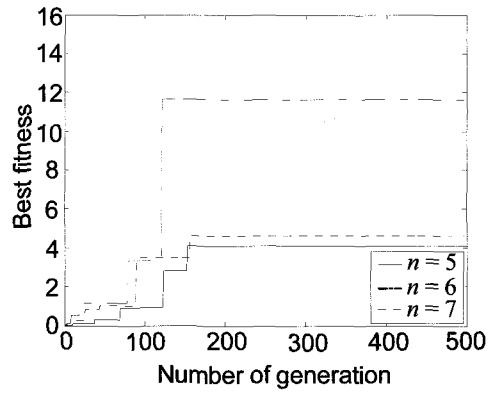

(a) solid ($n=5$), dash-dot ($n=6$), dotted ($n=7$)

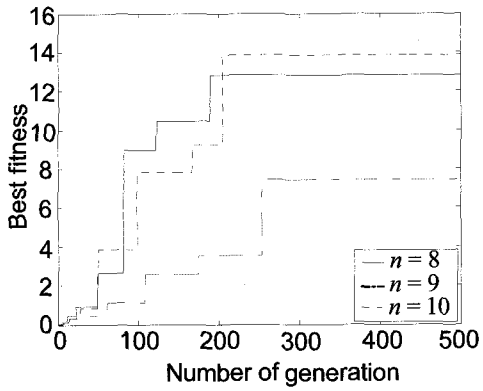

(b) solid ($n=8$), dash-dot ($n=9$), dotted ($n=10$)

FIG. 6. Best fitness with respect to the number of optical elements ($10^6\times\mu m^3$).

TABLE 3. Chromosomes corresponding to best fitnesses (mm)

n		C_0	C_1	C_2	C_3	C_4	C_5	C_6	C_7	C_8	C_9	C_{10}	l
5	f_k	0	60	250	∞	60	1.82						2
	$\overline{z}_k$	0	80	425	620	1035	1105						
6	f_k	0	120	60	250	∞	60	1.82					3
	$\overline{z}_k$	0	70	125	420	685	1105	1175					
7	f_k	0	60	200	∞	60	60	60	1.82				2
	$\overline{z}_k$	0	65	330	525	1000	1095	1180	1290				
8	f_k	0	60	150	100	100	250	∞	60	1.82			5
	$\overline{z}_k$	0	50	130	240	385	720	975	1400	1475			
9	f_k	0	60	200	∞	180	200	120	100	60	1.82		1
	$\overline{z}_k$	0	75	335	535	1000	1080	1170	1250	1335	1410		
10	f_k	0	150	100	120	250	100	150	200	∞	60	1.82	5
	$\overline{z}_k$	0	50	120	220	535	640	760	930	985	1405	1475	

distances (GD). Compared with Fig. 3, we could get that optimized optical layout that gives maximized workspace shows a shape of workspace like Fig. 3(a).

Table 5 shows the workspace dimensions obtained by changing the grid distances when n is ten. In Table 5, the amount of change of maximum workspace is very small when the grid distance of optical elements is smaller than 5 mm. Maximum workspace for the case when the grid distance of optical elements is 2.5 mm is increased by 0.57% compared to the case of 5 mm, but the case of 0.5 mm gives same maximum workspace as that of the case of 2.5 mm. This is because there is a limit of workspace dimensions that can be made by the combination of the optical element that are used. Since the smaller grid distance makes alignment difficult, we can say that 5 mm grid distance is

TABLE 4. Chromosomes obtained by changing the grid distances when n is ten (mm)

GD		C_0	C_1	C_2	C_3	C_4	C_5	C_6	C_7	C_8	C_9	C_{10}	l
10	f_k	0	60	150	150	250	60	180	180	∞	60	1.82	2
	$\overline{z}_k$	0	110	180	310	480	540	670	740	820	1240	1310	
2.5	f_k	0	60	250	150	150	180	150	250	∞	60	1.82	3
	$\overline{z}_k$	0	77.5	265	340	442.5	507.5	572.5	805	900	1322.5	1392.5	
0.5	f_k	0	60	250	150	150	180	150	250	∞	60	1.82	5
	$\overline{z}_k$	0	100	287.5	362.5	465	530	595	827.5	922.5	1345	1475	

TABLE 5. Workspace dimensions obtained by changing the grid distances when n is ten (μm)

	10	5	2.5	0.5
$\Delta d_z \mid_{\delta_i=-\delta,\phi_m=0}$	-79.09	-93.40	-99.91	-99.91
$\Delta d_z \mid_{\delta_i=+\delta,\phi_m=0}$	84.42	112.29	120.04	120.04
L_I	121.88	129.18	125.24	125.24
L_{II}	117.13	123.57	119.43	119.43
L_{III}	126.94	135.92	132.21	132.21
Max workspace ($10^6 \times \mu m^3$)	9.746	13.860	13.940	13.940

small enough to maximize the workspace of optical tweezers with a given pool of optical elements.

To verify the performance of our proposed method, we compared the result with previous study. In a previous report, Fallman *et al.* [8] designed a SLOT system that can move the focal point axially about 17 μm by 10 mm movement of lens and transversely about 2.5 μm by 1 mrad rotation of a mirror. To find the design solution, they derived system equation and analytically solved it by determining several design parameters. Thus they didn't allow that the beam at the OBA slightly changes in size and the cross section of a beam slightly deviates from the central axis to keep the same trapping efficiency. However, slight changes of the beam size and symmetry at the OBA decrease the trapping efficiency only slightly, because a similar degree of full beam power can be transmitted to the focal point, even if there were slight changes at the OBA. By slightly loosening the tight constraint of OT at the OBA by using the tolerance (ε), it can provide the optical layouts that give larger workspaces because it increases the possibility of finding the solutions that give larger workspace. Moreover, they considered the mechanical actuators to have an infinite moving range but this is not true. Thus they ignored the design solutions that can be made in a limited moving range even if these could produce larger movement of laser focus than the solution that they found. For this reason, their design solution was small under the given moving range of mechanical actuators. Table 6 shows the comparison of workspace when grid distance is 5 mm and n is six. Both longitudinal displacements and transverse displacements were increased with respect to the previous work, especially, about 4 times increase in lateral direction. Proposed method could achieve about 26 times increase in the size of workspace.

Figure 7 shows the variation of maximum workspace according to n. We increased the range of n from 3 to 16 to ascertain the influence of n with given optical table size. In the figure, when n is less than five, it does not yield large workspace. This is because it is difficult to make proper layout with only a few number of optical elements. On the other hand, maximum workspace decreases when n is greater than ten. This is because excessive number of optical elements crowds the layout space thus restricting possible solutions. When the number of optical elements is five through ten, the maximum workspace is relatively high. This means that there is an optimal number of optical elements for a given table length. But too many optical elements make the system alignment difficult. Therefore, one has to use a smaller number of optical elements even if the benefit is not as great.

TABLE 6. Comparison of workspace with previous work [8]

	Fallman (n=6)	Ours (n=6)
$\Delta d_z \mid_{\delta_i=-\delta,\phi_m=0}$	-84.52	-83.41
$\Delta d_z \mid_{\delta_i=+\delta,\phi_m=0}$	81.69	84.08
L_I	25.27	131.17
L_{II}	24.07	126.76
L_{III}	26.44	136.81
Max workspace ($10^6 \times \mu m^3$)	0.424	11.642

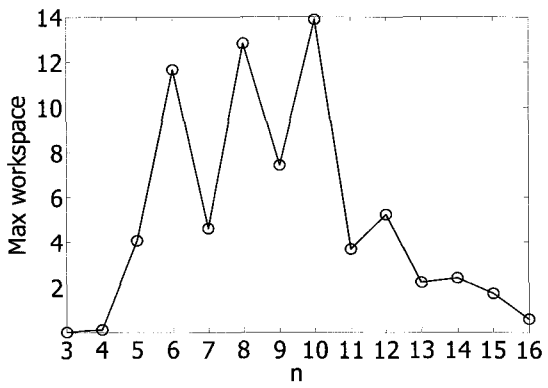

FIG. 7. Variation of maximum workspace with respect to n ($10^6 \times \mu m^3$).

IV. SUMMARY AND CONCLUSIONS

The workspace of optical tweezers where laser focus

can reach is design dependent and important factor in practical experiments. However, up to now, most researchers did not seriously consider the importance of workspace. In this paper, we proposed a new method for designing an optimized SLOT that gives maximized workspace with given pool of optical elements. For derivation of objective function, we applied ray tracing method with systematic approach. We allowed the beam at the OBA slight changes in size and symmetry because it barely decreases the trapping efficiency. From slightly loosening the tight constraint of OT at the OBA, we could find the optical layout that gives much larger workspace than for the previous study. In the experiment, we have shown that GA is effective in finding optimized SLOT layout that maximizes the workspace. The best layout giving the maximum workspace is searched by varying the number of optical elements and the grid distance between optical elements. We have shown that the amount of change of maximum workspace is very small when the grid distance of optical elements is smaller than 5 mm. Also, there is an optimal number of optical elements and grid distance for a given situation. Since too many optical elements make the system alignment difficult, in real experiment, one has to use smaller number of optical elements even if the benefit is not as great.

ACKNOWLEDGMENTS

This work was supported by the Research Center for Biomolecular Nanotechnology at GIST.

*Corresponding author: lygu@gist.ac.kr

REFERENCES

[1] A. Ashkin, J. M. Dziedzic, and T. Yamane, "Optical trapping and manipulation of single cells using infrared-laser beams," *Nature*, vol. 330, no. 6150, pp. 769-771, 1987.

[2] D. G. Grier, "A revolution in optical manipulation," *Nature*, vol. 424, no. 6950, pp. 810-816, 2003.

[3] K. Dholakia and P. Reece, "Optical micromanipulation takes hold," *Nanotoday*, vol. 1, no. 1, pp. 18-27, 2006.

[4] K. C. Neuman and S. M. Block, "Optical trapping," *Review of Scientific Instruments*, vol. 75, no. 9, pp. 2787-2810, 2004.

[5] B. A. Brown and P. R. Brown, "Optical tweezers: Theory and current applications," *American Laboratory*, vol. 33, no. 22, pp. 13-20, 2001.

[6] A. Ashkin, "Forces of a single-beam gradient laser trap on a dielectric sphere in the ray optics regime," *Biophysics Journal*, vol. 61, no. 2, pp. 569-582, 1992.

[7] V. Emiliani, D. Sanvitto, M. Zahid, F. Gerbal, and M. Coppey-Moisan, "Multi force optical tweezers to generate gradients of forces," *Optics Express*, vol. 12, no. 17, pp. 3906-3910, 2004.

[8] E. Fallman and O. Axner, "Design for fully steerable dual-trap optical tweezers," *Applied Optics*, vol. 36, no. 10, pp. 2107-2113, 1997.

[9] C. Mio, T. Gong, A. Terray, and D. W. M. Marr, "Design of a scanning laser optical trap for multiparticle manipulation," *Review of Scientific Instruments*, vol. 71, no. 5, pp. 2196-2200, 2000.

[10] S. U. Hwang and Y. G. Lee, "Topology optimization of optical tweezers setup," *Proc. of SPIE*, vol. 5650, pp. 408-417, Dec. 2004.

[11] I. Y. Park, S. U. Hwang, J. H. Song, and Y. G. Lee, "Grasping microscopic objects by an optical trapping system controlled by five finger tips," *Proc. of SPIE*, vol. 5930, pp. 59301Z-1, Aug. 2005.

[12] A. H. Forster, M. M. Wang, W. F. Butler, M. Chachisvilis, T. D. Y. Chung, S. C. Esener, J. M. Hall, O. Kibar, K. Lykstad, P. J. Marchand, E. M. Mercer, L. M. Pestana, S. Sur, E. Tu, R. Yang, H. Zhang, and I. Kariv, "Use of moving optical gradient fields for analysis of apoptotic cellular responses in a chronic myeloid leukemia cell model," *Analytical Biochemistry*, vol. 327, no. 1, pp. 14-22, 2004.

[13] M. M. Wang, C. A. Schnable, M. Chachisvilis, R. Yang, M. J. Paliotti, L. A. Simons, L. McMullin, N. Hagen, K. Lykstad, E. Tu, L. M. Pestana, S. Sur, H. Zhang, W. F. Butler, I. Kariv, and P. J. Marchand, "Optical forces for noninvasive cellular analysis," *Applied Optics*, vol. 42, no. 28, pp. 5765-5773, 2004.

[14] S. U. Hwang, I. Y. Park, J. H. Song, T. W. LeBrun, N. G. Dagalakis, C. Gagnon, A. Balijepalli, and Y. G. Lee, "Three-dimensional scanning optical tweezers," Proc. of SPIE, vol. 6048, pp. 604803, Dec. 2005.

[15] I. Ono, S. Kobayashi, and K. Yoshida, "Global and multi-objective optimization for lens design by real-coded genetic algorithms," *Proc. of SPIE*, vol. 3482, pp. 110-121, Sep. 1998.

[16] J. Beaulieu, C. Gagne, and M. Parizeau, "Lens system design and re-engineering with evolutionary algorithms," *Proc. of the Genetic and Evolutionary Computing Conference*, pp. 155-162, 2002.

[17] Y. Purushottam, R. V. H. Prasad, and V. C. Misra, "Design of ultra-wide band multilayer slant linear polarizer using a genetic algorithm," *Microwave and Optical Technology Letters*, vol. 30, no. 2, pp. 119-112, 2001.

[18] E. Kerrinckx, L. Bigot, M. Douay, and Y. Quiquempois, "Photonic crystal fiber design by means of a genetic algorithm," *Optics Express*, vol. 12, no. 9, pp. 1990-1995, 2004.

[19] D. Cojoc, E. D. Fabrizio, L. Businaro, S. Cabrinic, F. Romanatoa, and L. Vaccaria, "Design and fabrication of diffractive optical elements for optical tweezers arrays by means of e-beam lithography," *Microelectronic Engineering*, vol. 61-62, pp. 963-969, 2004.

[20] M. Gen and R. Cheng, *Genetic Algorithms and Engineering Design* (John Wiley & Sons, New Jersey, USA, 1997).

[21] F. L. Pedrotti and S. J. L. S. Pedrotti, *Introduction to Optics*, (Prentice Hall, New Jersey, USA, 1993) Chapter 4.

APPENDIX

A. System matrix

In ray optics, the height changes and angle changes can be expressed by linear equations. Figure 8 shows the progress of a single ray at optical elements. In the figure, 'k, k-1' denote current and previous index of element. Firstly, the height change between two adjacent elements in Fig. 8(a) can be described with a translation matrix. The translation matrix is,

$$\mathbf{T}_k = \begin{bmatrix} 1 & \overline{z}_k + \delta_k - \overline{z}_{k-1} - \delta_{k-1} & 0 \\ 0 & 1 & 0 \\ 0 & 0 & 1 \end{bmatrix} \quad , k = 1, 2, \cdots, n, \tag{11}$$

Thus, the height change between two adjacent elements is calculated as,

$$\mathbf{I}_k = \begin{bmatrix} h_k & \hat{h}_k \\ \alpha_k & \hat{\alpha}_k \\ 1 & 1 \end{bmatrix} = \mathbf{T}_k \mathbf{I}_{k-1} \quad , where \quad \mathbf{I}_{k-1} = \begin{bmatrix} h_{k-1} & \hat{h}_{k-1} \\ \alpha_{k-1} & \hat{\alpha}_{k-1} \\ 1 & 1 \end{bmatrix}. \tag{12}$$

Secondly, the angle changes at a thin lens or mirror is illustrated in Fig. 8(b-c) to describe the rotation matrix capable of representing lens and mirror at the same time. Motorized mirror that has ϕ rotation angle can rotate the beam optically two times that. Therefore, the rotation matrix for k th optical element can be represented as,

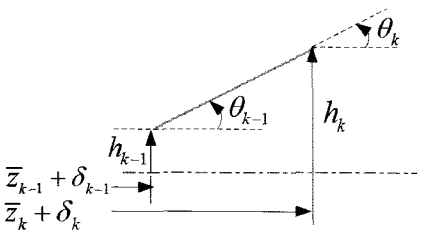

(a) Translation between two optical elements

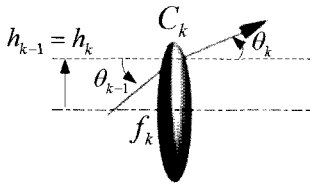

(b) Refraction at a thin lens

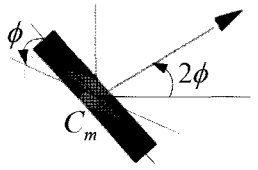

(c) Rotation at a motorized mirror

FIG. 8. Height and angle changes of a ray at optical elements.

$$\mathbf{R}_k = \begin{bmatrix} 1 & 0 & 0 \\ -1/f_k & 1 & 0 \\ 0 & 0 & 1 \end{bmatrix} \begin{bmatrix} 1 & 0 & 0 \\ 0 & 1 & 2\phi_k \\ 0 & 0 & 1 \end{bmatrix} = \begin{bmatrix} 1 & 0 & 0 \\ -1/f_k & 1 & 2\phi_k \\ 0 & 0 & 1 \end{bmatrix}. \tag{13}$$

Thus, the angle change between two adjacent elements is calculated as,

$$\mathbf{I}_k = \begin{bmatrix} h_k & \hat{h}_k \\ \alpha_k & \hat{\alpha}_k \\ 1 & 1 \end{bmatrix} = \mathbf{R}_k \mathbf{I}_{k-1} \quad , where \quad \mathbf{I}_{k-1} = \begin{bmatrix} h_{k-1} & \hat{h}_{k-1} \\ \alpha_{k-1} & \hat{\alpha}_{k-1} \\ 1 & 1 \end{bmatrix}. \tag{14}$$

Notice matrices in Eq. (11) and (13) can be used for both lenses and mirrors according to the selection of parameter values. Here, we would like to note some possible values for f_k, ϕ_k and δ_k in Table 7. If we constrain ourselves to commercially available optical elements, f_k is a discrete value for the case of a lens and an infinite value for the case of a mirror. Motorized rotation and motorized translation have 0 rotation angle for the lens and 0 displacement for the mirror. By combining rotation matrix and translation matrix, the system matrix is calculated as

$$\mathbf{M} = \mathbf{E}_n \mathbf{T}_n \cdots \mathbf{E}_1 \mathbf{T}_1 = \mathrm{F}(\phi_1, \cdots, \phi_n, f_1, \cdots, f_n, \overline{z}_0, \overline{z}_1 + \delta_1, \cdots, \overline{x}_n + \delta_n). \tag{15}$$

Thus the beam heights and angles at the objective lens can be obtained as

$$\mathbf{I}_n = \begin{bmatrix} h_n & \hat{h}_n \\ \alpha_n & \hat{\alpha}_n \\ 1 & 1 \end{bmatrix} = \mathbf{M}\mathbf{I}_0 \quad , where \quad \mathbf{I}_0 = \begin{bmatrix} h_0 & \hat{h}_0 \\ \alpha_0 & \hat{\alpha}_0 \\ 1 & 1 \end{bmatrix}. \tag{16}$$

B. Axial and lateral displacements

Figure 9 shows the schematic view when new position of the focal point is formed. In Fig. 9, new position of the focal point in the z direction is calculated by solving linear simultaneous equations of each boundary.

The linear equations are $\begin{cases} x = -\tan\theta_n \cdot z + h_n = -\alpha_n z + h_n \\ x = \tan\hat{\theta}_n \cdot z - \hat{h}_n = \alpha_n z - \hat{h}_n \end{cases}$.

By solving two linear equations, the new position of the focal point in the z direction is

$$d_z = \frac{h_n + \hat{h}_n}{\alpha_n + \hat{\alpha}_n}. \tag{17}$$

And the lateral displacement is calculated by substituting d_z into one of the linear equations above. The lateral displacement is

$$\Delta d_x = -\alpha_n \frac{h_n + \hat{h}_n}{\alpha_n + \hat{\alpha}_n} + h_n = \frac{h_n \hat{\alpha}_n - \hat{h}_n \alpha_n}{\alpha_n + \hat{\alpha}_n}. \tag{18}$$

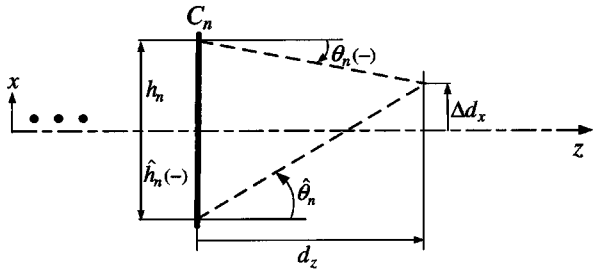

FIG. 9. Schematic view when new position of focal point is formed.